

NANO EXPRESS

Open Access

La_{1-x}Ca_xMnO₃ semiconducting nanostructures: morphology and thermoelectric properties

Mario Culebras^{*}, Raquel Torán, Clara M Gómez and Andrés Cantarero

Abstract

Semiconducting metallic oxides, especially perovskite materials, are great candidates for thermoelectric applications due to several advantages over traditionally metallic alloys such as low production costs and high chemical stability at high temperatures. Nanostructuring can be the key to develop highly efficient thermoelectric materials. In this work, La_{1-x}Ca_xMnO₃ perovskite nanostructures with Ca as a dopant have been synthesized by the hydrothermal method to be used in thermoelectric applications at room temperature. Several heat treatments have been made in all samples, leading to a change in their morphology and thermoelectric properties. The best thermoelectric efficiency has been obtained for a Ca content of $x = 0.5$. The electrical conductivity and Seebeck coefficient are strongly related to the calcium content.

Keywords: Nanostructures; Seebeck; Thermoelectricity; Perovskites

Background

Over the last decade, there has been an increasing interest in finding new highly efficient thermoelectric materials for electronic cooling [1-3] and power generation [4-6]. The energy demand in developed and under-developed countries is increasing due to the population growth and the improvement of the standard level of life in emerging countries. Unfortunately, reserves of fossil fuels are not unlimited, and their use generates huge amounts of CO₂ in the atmosphere. Many human activities (power plants, cement plants, steel mills, and vehicles engines as a few examples) are generating high amount of waste heat at different ranges of temperature. The conversion of this waste heat into electric energy would be an important contribution to the sustainable development as it would allow to reduce both the Greenhouse gas emissions and fossil fuel consumption. Thermoelectric generators are designed to convert a temperature difference into electricity (Seebeck effect) or, inversely, electric energy into a thermal gradient (Peltier effect). Thermoelectric materials must have a high conversion efficiency, and they must also be composed conveniently of non-toxic and abundantly available elemental species having high chemical stability in air. The

performance of a thermoelectric material is determined by the dimensionless figure of merit ZT :

$$ZT = \frac{\sigma S^2}{\kappa} T \quad , \quad (1)$$

S being the Seebeck coefficient, σ the electrical conductivity, κ the thermal conductivity, and T the absolute temperature. The power factor (PF) defined as $PF \equiv \sigma S^2$ can be used to compare the relative efficiency when the thermal conductivity is similar in different samples.

Over the past 30 years, semiconductor alloys based on Bi₂Te₃, PbTe, and SiGe [7-9] have been extensively studied and optimized for their use in thermoelectric applications. However, most of these compounds present disadvantages related to the shortage of raw materials, toxicity, or high costs of production.

For these reasons, research on the new materials to build up efficient thermoelectric devices is a scientific subject of current interest [10,11]. Recently, several oxides such as NaCoO₂ [12], Ca₃Co₄O₉ [13], Sr_{1-x}La_xTiO₃ [14], La_{1-x}Sr_xCoO₃ [15], Nd_{1-x}Ca_xCoO₃ [16], or Ca_{0.8}Dy_{0.2}MnO₃ [17] have shown excellent thermoelectric properties. More precisely, perovskite-type transition metal oxide single crystals have depicted large thermoelectric responses [14]. The electrical properties of

^{*}Correspondence: mario.culebras@uv.es
Materials Science Institute, University of Valencia, P. O. Box 22085, Paterna, Valencia, Spain

$\text{La}_{1-x}\text{A}_x\text{MnO}_3$ (A = Ca, Sr, Ba, and Pb) perovskite-type oxides are related to their stoichiometry [14]. Significant variations appear when the degree of substitution of the alkali-earth element for La varies from 0% to 50% [14]. The novelty of perovskite-type oxides is due to their low cost, non-toxicity, and possibility of being used for high-temperature applications. The origin of the thermoelectric properties in these oxides is not yet fully understood, but it could be related to the high spin-orbit interaction as well as the large electron effective mass [14].

In 1993, the work of Hicks and Dresselhaus [18] suggested that the morphology of a thermoelectric system can be used to improve both the electronic transport and the phonon scattering. Nanostructuring can increase ZT over unity by changing σ and S independently. The density of electronic states in a nanostructured system, when the Fermi energy is close to a maximum in the density of electronic states, depicts usually sharp peaks and theoretically larger Seebeck coefficients than the same material in bulk [19]. Furthermore, the phonon dynamics and heat transport in a nanostructured system can be suppressed by means of size effects. Nanostructures with one or more dimensions smaller than the phonon mean free path (a phonon glass) but larger than that of electrons (electron crystal) will noticeably reduce the thermal conductivity κ without affecting much the electrical transport. In other words, phonon transport will be strongly disturbed, while the electronic transport can remain bulk-like in nanostructured systems.

In this report, $\text{La}_{1-x}\text{Ca}_x\text{MnO}_3$ nanocrystals have been obtained by the hydrothermal method as a function of the Ca content. Several heat treatments have been made to determine the temperature when the perovskite phase is obtained. Scanning electron microscopy and X-ray diffraction studies have been used to determine the perovskite phase. The electrical conductivity and Seebeck coefficient have been determined as a function of temperature in order to analyze their thermoelectric performance.

Methods

Materials

The reactants $\text{MnCl}_2 \cdot 4\text{H}_2\text{O}$, $\text{Ca}(\text{NO}_3)_2$, $\text{La}(\text{NO}_3)_3$, KMnO_4 and KOH were purchased from Sigma Aldrich Co., Madrid, Spain.

Synthesis of $\text{La}_{1-x}\text{Ca}_x\text{MnO}_3$ nanostructures

$\text{La}_{1-x}\text{Ca}_x\text{MnO}_3$ samples with $x = 0.005, 0.05, 0.1$ and 0.5 have been prepared by a conventional hydrothermal treatment [20-22]. Stoichiometric amounts of reactants were used to have an aqueous solution of 0.55 M in cations (Mn^{7+} , Mn^{2+} , Ca^{2+} , and La^{3+}) by keeping a molar ratio

between KMnO_4 and $\text{MnCl}_2 \cdot 4\text{H}_2\text{O}$ according to the average valence of Mn ions in $\text{La}_{1-x}\text{Ca}_x\text{MnO}_3$. The pH of the solution was adjusted to 13 by adding KOH . After ultrasonic stirring, the solution was transferred into a Teflon autoclave and heated for 30 h at 230°C . Then, the reactor was cooled down to room temperature, and the obtained solid was washed with water and ethanol and dried at 230°C for 12 h. The powder was subjected to different temperatures, 650°C and 900°C for 12 h. The powder obtained after 900°C was pressed to form compact pellets (0.5-in. diameter) by using a pellet die at 490 MPa. Further, the pellet was sintered at 900°C for 24 h.

Characterization

The scanning electron microscopy (SEM) analysis was carried on a Hitachi 4800S microscope (Hitachi, Ltd., Tokyo, Japan) at an acceleration voltage of 20 kV and at a working distance of 14 mm for gold-coated surfaces. The wide-angle X-ray diffraction (WAXRD) patterns were acquired on a Bruker AXS D5005 diffractometer (Bruker AXS GmbH, Karlsruhe, Germany). The samples were scanned at $4^\circ/\text{min}$ using $\text{Cu K}\alpha$ radiation ($\lambda = 0.15418$ nm) at a filament voltage of 40 kV and a current of 20 mA. The diffraction scans were collected within the $2\theta = 20^\circ$ to 80° range with a 2θ step of 0.01° .

The electrical conductivity has been determined by means of the van der Pauw method [23,24], where four contacts are used to eliminate the effect of the contact resistance. The electrical conductivity can be obtained from two four-point resistance measurements independently either on contact resistances or on the specific geometry of the contact arrangement. For the first resistance measurement, a current I_{AC} is driven from two contacts, named A and C, and the potential difference V_{BD} between the other two contacts, B and D, was measured, giving the first resistance $R_1 = V_{BD}/I_{AC}$. The second resistance, $R_2 = V_{AB}/I_{CD}$, is obtained by driving the current from C to D and measuring the voltage between A and B. The conductivity of the sample is obtained by solving the van der Pauw equation:

$$e^{-\pi d R_1 \sigma} + e^{-\pi d R_2 \sigma} = 1 \quad , \quad (2)$$

where d is the sample thickness. A Keithley 2400 current source (Keithley Instruments Inc., Cleveland, OH, USA) was used as driving source.

The Seebeck coefficient has been measured with a homemade apparatus. In order to control the temperature, we used a Lakeshore 340 temperature controller, and to record the potential data, a Keithley 2750 Multime-

ter/Switching System was used. The Seebeck coefficient can be determined as the ratio between the electrical potential, ΔV , and the temperature difference, ΔT , that is,

$$S = \frac{\Delta V}{\Delta T} \quad (3)$$

Results and discussion

Scanning electron microscopy images show the evolution of the morphology as a function of temperature treatment (Figure 1A,B,C). The first temperature treatment was carried out at 230°C for 12 h (drying treatment); the resultant morphology after this treatment is shown in Figure 1C. A fibrillar morphology has been observed after this treatment, with an average diameter of 120 ± 50 nm. The second treatment was carried out at 650°C for 12 h, leading to a change in the morphology, from fibrillar to aggregated nanoparticles as shown in Figure 1B, although some parts of the powder retained the fibrillar morphology. Finally, the last treatment was carried out at 900°C for 12 h, as shown in Figure 1A; all the material depicts a nanoparticle structure. This evolution of the morphology with temperature is similar to that observed in others materials like $\text{La}_{1-x}\text{Sr}_x\text{CoO}_3$, previously reported in the literature [25].

The X-ray diffraction patterns for the $\text{La}_{1-x}\text{Ca}_x\text{MnO}_3$ ($x = 0.05$) powder, resulting from the thermal treatment

at 230°C, 650°C, and 900°C are depicted in Figure 1D. Similar diffraction patterns are obtained for all the samples regardless the Ca content. X-ray diffraction analysis has been made in order to know when the orthorhombic perovskite phase appears because only this phase presents thermoelectric activity [26-28]. At 230°C, the perovskite phase was not obtained, resulting in an insulating material. The diffraction peaks observed at 230°C are related to segregated metallic oxides of Ca, La, and Mn (CaO , Mn_3O_4 , CaMn_2O_4 , etc.). At 650°C, the WAXDR spectrum indicates that the orthorhombic perovskite-type structure is present. The material obtained after this treatment was a semiconductor material. The WAXDR spectrum of the sample heated at 900°C is similar to that obtained at 650°C, indicating that most of the material has the perovskite phase. The perovskite phase is attained at 650°C; however, the electrical conductivity of the compacted powder (without sintering) obtained at 650°C and 900°C is very low (around 10^{-3} S/cm). In addition, the sample size and shape are more homogeneous after treatment at 900°C. Thus, in order to use these materials for thermoelectric applications, we have realized a sintering process by keeping the compact pellet at 900°C for 24 h.

The electrical conductivity of the samples after the sintering process is plotted in Figure 2A. An increase of 3 orders of magnitude with respect to the samples before the sintering process is observed. This fact can be explained

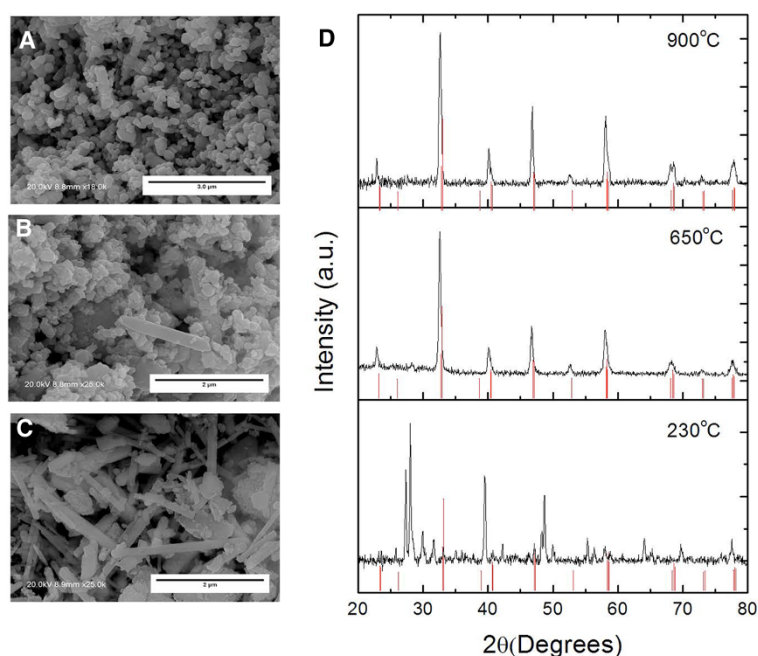
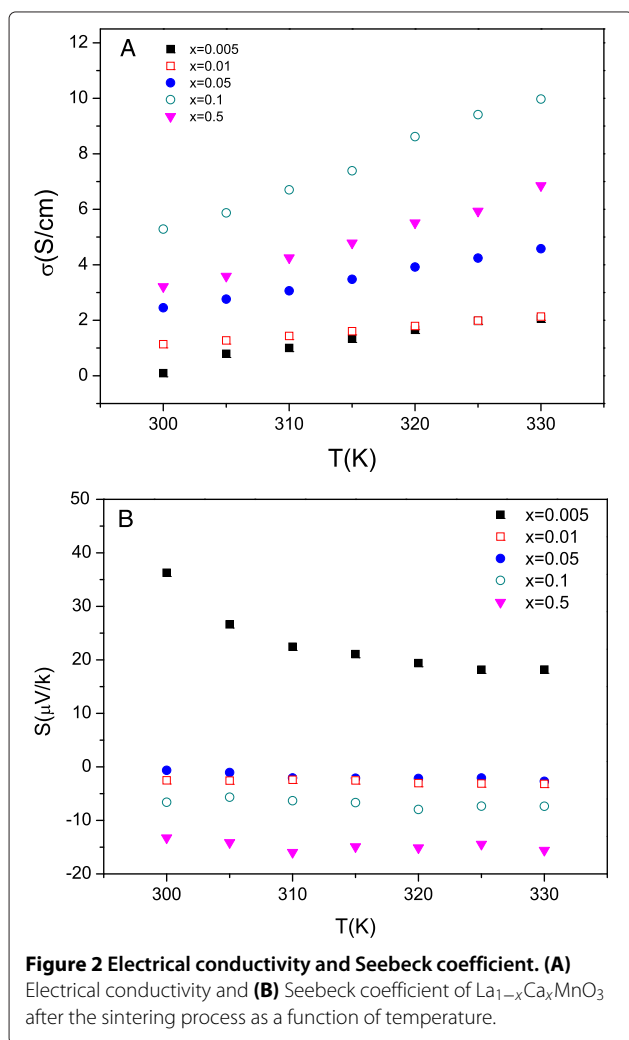


Figure 1 Scanning electron microscopy images after different temperature treatments for 12 h. (A) 900°C, (B) 650°C, and (C) 230°C. (D) X-ray diffraction spectra of $\text{La}_{1-x}\text{Ca}_x\text{MnO}_3$ nanostructures ($x = 0.05$). The red lines refer to the perovskite phase diffraction pattern.



by the reduction of the interfaces and grain boundaries during the sintering process. The electrical conductivity increases with temperature; this trend is expected in semiconducting materials [29,30]. The maximum value of the electrical conductivity, 10 S/cm, has been obtained for $\text{La}_{0.9}\text{Ca}_{0.1}\text{MnO}_3$ at 330 K. The increase of the calcium content in the nanostructured material produces an enhancement of the electrical conductivity, with the exception of $\text{La}_{0.5}\text{Ca}_{0.5}\text{MnO}_3$. Figure 2B shows the variation of the Seebeck coefficient with the temperature and Ca content. The values of S change from positive to negative at high Ca content, denoting a change from p-type to n-type conduction. The dependence of S with temperature is negligible except for the lower Ca content ($x = 0.005$).

Generally, a p-type conductivity is observed in LaMnO_3 [31,32]. It has been attributed to the excess of oxygen ($\text{O}_{3+\delta}$) and La vacancies and probably also to Mn vacancies [33], although it is not completely clear. Doing a

literature search, it is clear that LaMnO_3 is a p-type semiconductor, while CaMnO_3 is an n-type semiconductor and contains an oxygen defect ($\text{O}_{3-\delta}$). In the work of Zeng et al. [34], electrical conductivity is analyzed as a function of the oxygen defect and they obtain a decrease of the activation energy as soon as the defect of oxygen is higher. From these observations, we can argue that the type of conduction in $\text{La}_{1-x}\text{Ca}_x\text{O}_3$ goes from p to n as soon as the Ca content increases. We have found in our measurements that only the sample with $x = 0.005$ is a p-type semiconductor, while all the samples with a higher Ca concentration are n-type semiconductors. There are several empirical models in the literature [27,33] to explain the conductivity based on different vacancies, but the location of the Mn(d) and O(p) levels is not clear. There are also several *ab initio* calculations, but we have found contradictions in the location of the Mn(d) and O(p) levels, probably due to the Jan-Teller distortion.

The power factor has been calculated in order to estimate the thermoelectric efficiency in this kind of materials at 330 K (Table 1). The best power factor, $0.16 \mu\text{W m}^{-1} \text{K}^{-2}$ has been reached in the $\text{La}_{0.5}\text{Ca}_{0.5}\text{MnO}_3$ sample. The values estimated in this work are similar to those found in organic semiconductors [35-37].

Conclusions

$\text{La}_{1-x}\text{Ca}_x\text{MnO}_3$ perovskite nanostructures have been synthesized by the hydrothermal method. The perovskite-type structure has been obtained at 650°C and 900°C . The nanostructure morphology changes from fibrillar to nanoparticle type when increasing the temperature treatment. The electrical conductivity increases 3 orders of magnitude after the sintering process. The electrical conductivity depends on the calcium content. The sign of Seebeck coefficient changes from positive to negative. The best power factor of $0.16 \mu\text{V/mK}^2$ has been obtained for the sample $\text{La}_{0.5}\text{Ca}_{0.5}\text{MnO}_3$. The magnitude of PF indicates that these materials have a modest efficiency at room temperature. More research is needed in order to increase the thermoelectric efficiency.

Table 1 Thermoelectric parameters of $\text{La}_{1-x}\text{Ca}_x\text{MnO}_3$ nanostructures at 330 K

Sample	σ (S/cm)	S ($\mu\text{V/K}$)	Power factor ($\mu\text{W/mK}^2$)
$\text{La}_{0.995}\text{Ca}_{0.005}\text{MnO}_3$	2.05	18.18	0.068
$\text{La}_{0.99}\text{Ca}_{0.01}\text{MnO}_3$	2.13	-2.69	0.002
$\text{La}_{0.95}\text{Ca}_{0.05}\text{MnO}_3$	4.57	-3.18	0.003
$\text{La}_{0.9}\text{Ca}_{0.1}\text{MnO}_3$	10.00	-7.35	0.053
$\text{La}_{0.5}\text{Ca}_{0.5}\text{MnO}_3$	6.85	-15.577	0.166

Competing interests

The authors declare that they have no competing interests.

Authors' contributions

MC was in charge of the thermoelectric characterization, RT developed the synthesis of materials, CMG was in charge of X-ray analysis, and AC realized the discussion of the thermoelectric results. All authors read and approved the final manuscript.

Acknowledgements

We acknowledge the financial support of the Ministry of Finances and Competitiveness through the Grant CDS2010-0044 belonging to the 'Consolider-Ingenio Programme', Grant MAT2012-33483, and the FPU Programme for young researchers.

Received: 14 May 2014 Accepted: 7 July 2014

Published: 21 August 2014

References

- Kim M-Y, Oh T-S: **Thermoelectric power generation characteristics of a thin-film device consisting of electrodeposited n-Bi₂Te₃ and p-Sb₂Te₃ thin-film legs.** *J Electron Mater* 2013, **42**(9):2752–2757.
- Zhao D, Tan G: **A review of thermoelectric cooling: materials, modeling and applications.** *Appl Therm Eng* 2014, **66**(1–2):15–24.
- Sharma S, Dwivedi VK, Pandit SN: **Exergy analysis of single-stage and multi stage thermoelectric cooler.** *Int J Energy Res* 2014, **38**(2):213–222.
- Yoon CK, Chitnis G, Ziaie B: **Impact-triggered thermoelectric power generator using phase change material as a heat source.** *J Micromech Microeng* 2013, **23**(11):114004.
- Jo S-E, Kim M-S, Kim M-K, Kim Y-J: **Power generation of a thermoelectric generator with phase change materials.** *Smart Mater Struct* 2013, **22**(11):115008.
- Hourdakis E, Nassiopoulou AG: **A thermoelectric generator using porous Si thermal isolation.** *Sensors* 2013, **13**(10):13596–13608.
- Saleemi M, Toprak MS, Li S, Johnsson M, Muhammed M: **Synthesis, processing, and thermoelectric properties of bulk nanostructured bismuth telluride (Bi₂Te₃).** *J Mater Chem* 2012, **22**(2):725–730.
- Semizorov A: **A study of pressed thermoelectric-materials based on Bi₂Te₃-Sb₂Te₃-Sb₂Se₃ solid-solutions.** *Inorg Mater* 1995, **31**(6):675–677.
- Hasapis TC, Girard SN, Hatzikraniotis E, Paraskevopoulos KM, Kanatzidis MG: **On the study of PbTe-based nanocomposite thermoelectric materials.** *J Nano Res* 2012, **17**:165–174.
- Ghraiiri N, Bouaicha M: **Structural, morphological, and optical properties of TiO₂ thin films synthesized by the electrophoretic deposition technique.** *Nanoscale Res Lett* 2012, **7**:357.
- Mula G, Manca L, Setzu S, Pezzella A: **Photovoltaic properties of PSI impregnated with eumelanin.** *Nanoscale Res Lett* 2012, **7**(1):1–9.
- Terasaki I, Sasago Y, Uchinokura K: **Large thermoelectric power in NaCo₂O₄ single crystals.** *Phys Rev B* 1997, **56**:12685–12687.
- Masset A, Michel C, Maignan A, Hervieu M, Toulemonde O, Studer F, Raveau B, Hejtmanek J: **Misfit-layered cobaltite with an anisotropic giant magnetoresistance: Ca₃Co₄O₉.** *Phys Rev B* 2000, **62**(1):166–175.
- Okuda T, Nakanishi K, Miyasaka S, Tokura Y: **Large thermoelectric response of metallic perovskites: Sr_{1-x}La_xTiO₃ (0 < x < 0.1).** *Phys Rev B* 2001, **63**:113104.
- Berggold K, Kriener M, Zobel C, Reichl A, Reuther M, Müller R, Freimuth A, Lorenz T: **Thermal conductivity, thermopower, and figure of merit of La_{1-x}Sr_xCo₃.** *Phys Rev B* 2005, **72**:155116.
- Culebras M, Gomez C, Gomez A, Sapina F, Cantarero A: **Synthesis of Nd_{1-x}Ca_xCoO₃ perovskite nanowires for thermoelectric applications.** *J Elect Eng*, 2:59–64.
- Park K, Lee GW: **Thermoelectric properties of Ca_{0.8}Dy_{0.2}MnO₃ synthesized by solution combustion process.** *Nanoscale Res Lett* 2011, **6**:548.
- Hicks LD, Dresselhaus MS: **Effect of quantum-well structures on the thermoelectric figure of merit.** *Phys Rev B* 1993, **47**(19):12727–12731.
- Humphrey TE, Linke H: **Reversible thermoelectric nanomaterials.** *Phys Rev Lett* 2005, **94**:096601.
- Wang Y, Fan HJ: **Improved thermoelectric properties of La_{1-x}Sr_xCoO₃ nanowires.** *J Phys Chem C* 2010, **114**(32):13947–13953.
- Zhang T, Jin C, Qian T, Lu X, Bai J, Li X: **Hydrothermal synthesis of single-crystalline La_{0.5}Ca_{0.5}MnO₃ nanowires at low temperature.** *J Mater Chem* 2004, **14**(18):2787–2789.
- Zhu X, Wang J, Zhang Z, Zhu J, Zhou S, Liu Z, Ming N: **Perovskite nanoparticles and nanowires: microwave-hydrothermal synthesis and structural characterization by high-resolution transmission electron microscopy.** *J Am Ceram Soc* 2008, **91**(8):2683–2689.
- Van Der Pauw LJ: **A method of measuring the resistivity and Hall coefficient on lamellae of arbitrary shape.** *Philips Tech Rev* 1958, **20**:220–224.
- de Boor J, Schmidt V: **Complete characterization of thermoelectric materials by a combined van der Pauw approach.** *Adv Mater* 2010, **22**(38):4303–4307.
- Deng J, Zhang L, Dai H, He H, Au CT: **Single-crystalline La_{0.6}Sr_{0.4}CoO_{3-δ} nanowires/nanorods derived hydrothermally without the use of a template: catalysts highly active for toluene complete oxidation.** *Catal Lett* 2008, **123**(3–4):294–300.
- Mahendiran R, Tiwary S, Raychaudhuri A, Ramakrishnan T, Mahesh R, Rangavittal N, Rao C: **Structure, electron-transport properties, and giant magnetoresistance of hole-doped LaMnO₃ systems.** *Phys Rev B* 1996, **53**(6):3348–3358.
- Mizusaki J, Yonemura Y, Kamata H, Ohyama K, Mori N, Takai H, Tagawa H, Dokiya M, Naraya K, Sasamoto T, Inaba H, Hashimoto T: **Electronic conductivity, Seebeck coefficient, defect and electronic structure of nonstoichiometric La_{1-x}Sr_xMnO₃.** *Solid State Ion* 2000, **132**(3–4):167–180.
- Shimura T, Hayashi T, Inaguma Y, Itoh M: **Magnetic and electrical properties of La(y)A(x)Mn(w)O(3) (A=Na, K, Rb, and Sr) with perovskite-type structure.** *J Solid State Chem* 1996, **124**(2):250–263.
- Huang XY, Miyazaki Y, Kajitani T: **High temperature thermoelectric properties of Ca_{1-x}Bi_xMn_{1-y}V_yO_{3-δ} (0 ≤ x = y ≤ 0.08).** *Sol State Commun* 2008, **145**(3):132–136.
- Koc R, Anderson H: **Electrical conductivity and Seebeck coefficient of (La, Ca)(Cr, Co)O₃.** *J Mater Sci* 1992, **27**(20):5477–5482.
- Kuo J, Anderson H, Sparlin D: **Oxidation reduction behavior of undoped and Sr-doped LaMnO₃: defect structure, electrical conductivity, and thermoelectric power.** *J Solid State Chem* 1990, **87**(1):55–63.
- Ritter C, Ibarra M, DeTeresa J, Algarabel P, Marquina C, Blasco J, Garcia J, Oseroff S, Cheong S: **Influence of oxygen content on the structural, magnetotransport, and magnetic properties of LaMnO₃+δ.** *Phys Rev B* 1997, **56**(14).
- Mizusaki J, Mori N, Takai H, Yonemura Y, Minamiue H, Tagawa H, Dokiya M, Inaba H, Naraya K, Sasamoto T, Hashimoto T: **Oxygen nonstoichiometry and defect equilibrium in the perovskite-type oxides La_{1-x}Sr_xMnO₃.** *Solid State Ion* 2000, **129**(3–4):163–177.
- Zeng Z, Greenblatt M, Croft M: **Large magnetoresistance in antiferromagnetic CaMnO₃-δ.** *Phys Rev B* 1999, **59**(13):8784–8788.
- Taylor PS, Korugic-Karasz L, Wilusz E, Lahti PM, Karasz FE: **Thermoelectric studies of oligophenylenevinylene segmented block copolymers and their blends with MEH-PPV.** *Synth Met* 2013, **185**:109–114.
- Shi H, Liu C, Xu J, Song H, Lu B, Jiang F, Zhou W, Zhang G, Jiang Q: **Facile fabrication of PEDOT:PSS/polythiophenes bilayered nanofilms on pure organic electrodes and their thermoelectric performance.** *ACS Appl Mater Interfaces* 2013, **5**(24):12811–12819.
- Yoon C, Kim J, Sung H, Lee H: **Electrical conductivity and thermopower of phosphoric acid doped polyaniline.** *Synth Met* 1997, **84**(1–3):789–790.

doi:10.1186/1556-276X-9-415

Cite this article as: Culebras et al.: La_{1-x}Ca_xMnO₃ semiconducting nanostructures: morphology and thermoelectric properties. *Nanoscale Research Letters* 2014 **9**:415.